Effect of fiber array irregularities on microscopic interfacial normal stress states of transversely loaded UD-CFRP from viewpoint of failure initiation

AUTHOR(S):

Hojo, Masaki; Mizuno, Masaaki; Hobbiebrunken, Thomas; Adachi, Taiji; Tanaka, Mototsugu; Ha, Sung Kyu

CITATION:

Hojo, Masaki ...[et al]. Effect of fiber array irregularities on microscopic interfacial normal stress states of transversely loaded UD-CFRP from viewpoint of failure initiation. Composites Science and Technology 2009, 69(11-12): 1726-1734

ISSUE DATE:

2009-09

URL:

http://hdl.handle.net/2433/80168

080823v263

Effect of fiber array irregularities on microscopic interfacial normal stress states of transversely loaded UD-CFRP from viewpoint of failure initiation

Masaki HOJO[1,5], Masaaki MIZUNO[1], Thomas HOBBIEBRUNKEN[1,4], Taiji ADACHI[1], Mototsugu TANAKA[2], and Sung Kyu HA[3]

1 Department of Mechanical Engineering and Science, Kyoto University, Sakyo-ku, Kyoto 606-8501, Japan

2 Department of Aeronautics, Kanazawa Institute of Technology, Ohgigaoka, Nonoichi, Ishikawa 921-8501, Japan

3 Department of Mechanical Engineering, Hanyang University, Sangrok-gu, Ansan-shi, Gyeonggi-do 426-791, Korea

4 Present affiliation and address: Airbus Deutschland, 28199 Bremen, Germany

5 Corresponding author

E-mail address: hojo_cm@mech.kyoto-u.ac.jp

Tel.: +81-75-753-4836, Fax: +81-75-771-7286

Abstract

A detailed investigation has been carried out to determine the effect of local fiber array irregularities and controlling fiber distribution parameters on microscopic interfacial normal stress states for transversely-loaded unidirectional carbon fiber (CF)/epoxy composites. Linear elastic finite element analyses were carried out for two-dimensional image-based models composed of about 70 fibers. The relationship between the geometrical distribution of two adjacent fibers and the interfacial normal stresses (INSs) is

investigated for all fibers in different image-based models. Three boundary conditions for loading were selected: Case A involved cooling from the curing temperature (the difference in temperature was -155 K); Case B involved transverse loading of 75 MPa chosen as an example of macroscopic transverse fracture strength; and Case C involved both cooling from the curing temperature and transverse loading of 75 MPa. High compressive INSs due to the difference in the coefficients of thermal expansion are observed at the location of the shortest interfiber distance for Case A (cooling). High tensile INSs are observed at the location of the shortest interfiber distance and where the fiber alignment angle to the loading direction is small for Case B (loading). For Case C (cooling and loading), the high thermal residual compressive INSs and the high mechanical tensile INSs compensate each other, and the INSs at a short interfiber distance are much lower than those for Case B. These results clearly indicate the importance of the contribution of the thermal residual stresses to the transverse tensile failure initiation of CF/epoxy laminates.

Key words: B. Debonding; C. Finite element analysis (FEA); C. Transverse cracking; C. Residual stress; Micromechanics

1. Introduction

Transverse fracture is often the first failure mechanism that occurs early in the loading stage of composite structures [1-3]. The transverse fracture strain, 0.5 to 1 %, is often much smaller than that of neat resin [4-6]. This transverse fracture strain is smaller than that in the fiber direction and is the major factor for determining the limiting strain in the design of carbon fiber reinforced plastics (CFRP) structures [7]. The mechanisms of initial transverse fracture are characterized as localized deformation and fracture of the matrix and interface [8]. The interfacial strength has a significant influence on the transverse failure of composites [9,10]. Several previous studies on CFRP have demonstrated the positive effects of interfacial adhesion on the onset strain of transverse failure [9-12]. Our

previous in situ experiments revealed that interfacial fracture was the dominant mechanism for transversely loaded carbon fiber (CF)/epoxy laminates [13]. The mesoscopic interfacial stresses at the initiation of fracture were determined by micro/macro finite element analysis with a periodic fiber arrangement and were compared with the in situ experimental results. The results showed that the interfacial normal stress (INS) controls the onset of transverse failure at the interface. The failure was observed at the location where the interfiber distance was smallest and the alignment of the related two fibers was in the loading direction. The thickness of resin at the location where failure occurred was about 0.5 to 1 μm. It is interesting to note that fibers do not touch each other at this point. The onset of fracture at the interface was also reported for glass fiber composites [1,14].

As far as macroscopically measured elastic properties are concerned, the assumption of periodic fiber arrangement does not cause significant error [15,16]. Sun and Vaidya [15] analyzed a representative volume element to predict macroscopic composite properties using regular fiber arrays, such as square and hexagonal arrays. On the other hand, failure initiation is a result of the microscopic stress and strain states. Most of the previous numerical studies have used regular fiber arrays to investigate complex microscopic stress and strain states caused by mechanical and thermal loadings [10,11,17,18]. However, it is important to know how microscopic stress and strain distributions are affected by the local fiber distribution.

Earlier works on this subject focused mainly on thermal residual stresses. Fletcher and Oakeshott [19] investigated the effect of interfiber distance on thermal residual stresses using regular fiber arrays. Sørensen and Talreja [20] have carried out pioneering and systematic researches on the effects of nonuniformity of fiber distribution on thermally-induced residual stresses and cracking in ceramic matrix composites. They studied the nonuniformity parameters such as interfiber distance, fibers in contact, and fiber- and matrix-rich region using several configurations of fiber arrangement. They found that the radial stress component at the fiber/matrix interface is most affected by the

nonuniformity parameters, attaining a peak compressive value at the point of contact between fibers.

In recent works it has been shown that the irregular fiber microstructure has a great influence on microscopic stress states and damage evolution. Fiedler et al. [21] studied the influence of the local fiber volume fraction on the composite transverse strength using a hexagonal unit cell model. Fletcher and Oakeshott [22] investigated the distribution of tangential stress at the fiber/matrix interface using random fiber arrays under thermal loading. Nakamura and Suresh [23] investigated the macroscopic nonlinear stress-strain behavior of metal matrix composites using irregular fiber arrays. Although Bulsara et al. [24] investigated the damage initiation for unidirectional ceramic matrix composites, they only considered the results statistically. Ha and coauthors [25,26] statistically investigated the fiber/matrix interfacial stress distribution of CF/epoxy using irregular fiber arrays under mechanical and thermal loadings. Thus, only limited information is available on the effect of irregular fiber distribution on microscopic mechanical and thermal residual stress states. In particular, the relationship between the detailed local geometrical fiber arrangement and the distribution of microscopic stress states and their relation to the failure initiation are still unknown.

Another important aspect that should be taken into account is the triaxial stress sate of the matrix resin. The matrix strength greatly depends on the stress state [27-29]. Asp et al. have carried out systematic studies on the strength of epoxy resin subjected to triaxial stress states and its relation to failure initiation for transversely loaded glass fiber/epoxy composites [17,18,30,31]. They focused on failure initiation in the matrix for composites with a strong and tough fiber/matrix interface. They first dealt with a criterion for crack initiation in glassy polymers subjected to a composite-like stress state [30,31]. Then, they showed that the failure criterion of transversely loaded glass fiber/epoxy composites is dilatation energy or the hydrostatic stress [17,18].

In the present study, a detailed numerical investigation has been carried out to

determine the influences of the interfiber distance and the fiber alignment angle to the loading direction on the microscopic interfacial normal stress (INS) states for thermally and transversely loaded CF/epoxy. The role of thermal residual stress was discussed from the viewpoint of failure initiation. Here, we only focused on INS as a first step, and the consideration of the triaxial stress [17,18,30,31] can be the next step of the study.

2. Numerical analysis

A finite element software, Marc (version 2003), was used in the present analysis. The two-dimensional image-based models of 70 μm x 70 μm are made on the basis of the scanning electron micrographs of transverse section of HTA/RTM6 laminates [13] as shown in Fig. 1(a). The three models used in the present study are composed of about 70 fibers, and their volume fraction of fibers is 62%. These are named as Model 1, 2 and 3, and Model 1 is only shown in Fig. 1(b). Here, the fiber surface is indicated by thick lines. Fibers with solid lines indicate that fibers are perfectly inside the model, and those with dashed lines indicate that fiber surface crosses the boundary of the model. In each model, differences between individual fiber diameters are taken into account, and the average diameter and the standard deviation are 6.9 μm and 0.25 μm, respectively. Though actual fiber cross sections are not exact circles, the fibers in the models are slightly modified to have perfect circular cross sections with the same sectional area as that of the original fibers. Fig. 1(c) indicates an enlarged part of Model 1. Fine meshes are used at the fiber surfaces and interfiber regions. Four node rectangular elements are mainly used, and three node triangle elements are used for limited position. Each fiber surface is divided into 64 rectangular elements. The total number of elements for each model is about 35000. Fig. 2 shows field emission scanning electron micrographs (FE-SEMs) of a local part of the transverse cross section of HTA/RTM6 where two fibers are almost touching. A surface roughness of 30 to 60 nm is observed for the carbon fiber. A thin resin layer is clearly observed between the two fibers in the cross section. These interfiber distances are

approximately 30 to 90 nm. Thus, the shortest interfiber distance is determined as 30 nm in the analytical models. Since the stress state at the fiber/matrix interface is not singular or highly concentrated, only one or two elements are placed at the interfiber position for the case of 30 nm interfiber distance as shown in Fig. 1(c). The accuracy of the calculation was validated by using the models with finer meshes of two and ten elements at the same interfiber position. Only linear elastic plane strain analyses were carried out. The parameters used in this calculation are obtained from CF supplier and references, and they are tabulated in Table 1 [1,16,32].

Fig. 3 shows the boundary conditions used for the finite element analyses. Three boundary conditions for loading are selected. Case A involves cooling from the curing temperature (453 K) to room temperature (298 K). Here, the change in temperature, ΔT, is -155 K. Case B involves transverse loading of 75 MPa in the direction of x_1 axis. This stress is selected as an example of macroscopic transverse fracture strength for HTA/RTM6 [13]. Case C involved both cooling and loading under above conditions (Cases A and B). In the present study, only the interfacial normal stresses (INSs) of all fibers are calculated because our previous in situ study showed that this component is critical for the onset of the fiber/matrix interfacial failure of transversely loaded layers [13]. The INS at each node on the fiber surface is calculated from the average of the stress tensor of the two adjacent integration points in the matrix.

Fig. 4 shows schematics of the two models used that consist of regular hexagonal arrays with different loading directions in which the fiber diameter is 6.9 μm and the volume fraction of fiber is 60%. These two hexagonal models (Hex 1 and 2) are also used in the calculation under the same boundary conditions for comparison. The zero degree corresponds the loading direction.

3. Results and discussion

3.1 Periodic hexagonal array

Fig. 5 shows the calculated results of INSs for the periodic hexagonal arrays under the three different boundary conditions, Cases A, B and C. For Case A (cooling) shown in Fig. 5(a), the minimum INSs of -10 MPa are repeatedly occurring at the shortest interfiber distance, i.e. every 60˚ starting at 0˚. The maximum INSs of 0 MPa are occurring at the resin rich zone, i.e. every 60˚starting at 30˚. Compressive INSs are generally observed, and the location of the minimum value along the circumference is strongly affected by the nearest neighboring fibers for Case A (cooling).

Fig. 5(b) shows the results of Hex 1 and 2 for Case B (loading). For Hex 1 (fibers are aligned in the loading direction), the maximum tensile INSs of 120 MPa are located at θ = 0˚ and 180˚, which correspond to the shortest interfiber distance in the loading direction. The minimum INSs of 3 MPa are located at θ = 60˚, 120˚, 240˚, 300˚, which correspond to the shortest interfiber distance apart from in the loading direction. Small peaks of 16 MPa are also located at θ = 90˚ and 270˚, which correspond to the resin-rich part far from the loading direction. For Hex 2 (fibers are aligned 30˚ to the loading direction), the maximum INSs of 80 MPa are located at θ = 30˚, 150˚, 210˚, 330˚, which correspond to the shortest interfiber distance near the loading direction. The INSs in the loading direction, i.e. at θ = 0˚ and 180˚, are 60 MPa, and this value is slightly smaller than the maximum value. The minimum INSs of -30 MPa are located at θ = 90˚ and 270˚, which correspond to the shortest interfiber distance perpendicular to the loading direction. Thus, the maximum INSs are strongly affected by the closest neighboring fibers near the loading direction for both Hex 1 and 2 for Case B (loading), and this is due to the direct stress flow in the loading direction. The minimum INSs are also affected by the closest neighboring fibers far from the loading direction for both Hex 1 and 2, and this is due to Poisson’s contraction effect.

Fig. 5(c) shows the results of Hex 1 and 2 for Case C (cooling and loading). The general trend is similar to that for Case B. In fact, Case C is a superposition of Cases A and B. Since the minimum INSs for Case A, and the maximum INSs for Case B are located in

the direction of the shortest interfiber distance, these two extreme values compensate each other and the maximum INSs for Case C are smaller than those for Case B. The maximum tensile INSs of 110 MPa are located at θ = 0˚ and 180˚ for Hex 1 (fibers are aligned in the loading direction), and those of 70 MPa are located at θ = 30˚, 150˚, 210˚, 330˚ for Hex 2 (fibers are aligned 30˚ to the loading direction). For Hex 1, the minimum INSs of -5 MPa are located at θ = 60˚, 120˚, 240˚, 300˚, and small peaks of 17 MPa are also located at θ = 90˚ and 270˚. For Hex 2, the INSs in the loading direction, i.e. at θ = 0˚ and 180˚, are 60 MPa, and the minimum INSs of -50 MPa are located at θ = 90˚ and 270˚. Since the maximum INSs due to mechanical loading and the minimum INSs due to thermal loading compensate each other at the location of the shortest interfiber distance on the circumference, a similar trend should be counted carefully for the case of irregular fiber arrays where the shortest interfiber distance is much smaller than that of a periodic hexagonal array.

3.2 Irregular fiber arrays – General views

Fig. 6 shows enlarged fibers of Model 1 for Cases A, B and C with INS contour. Similar results are obtained for Models 2 and 3. For Case A (cooling), high minimum compressive INSs of -120 to -100 MPa are occurring where two fibers are almost touching, as indicated by red circles. Maximum tensile INSs of 20 MPa are occurring at the resin-rich zone. The minimum INSs for irregular fiber arrays are much smaller than those for the periodic hexagonal array, and the maximum INSs for irregular arrays are higher than those for the periodic hexagonal array, respectively. The difference between the maximum and minimum INSs for irregular arrays (about 140 MPa) is thus much larger than that for the periodic hexagonal array (about 10 MPa).

For Case B (loading), high maximum tensile INSs of 180 to 190 MPa are occurring where two fibers are almost touching, and these two fibers are nearly parallel to the loading direction (the interfaces are nearly normal to the loading direction), as indicated by the red

circles. The location of the maximum INSs are more directly affected by the interfiber distance than by the angle to the loading direction, and the maximum INSs for each fiber are occurring where two fibers are almost touching and are aligned at an angle (less than 30˚) to the loading direction, as indicated by red dashed circles. This fact agrees well with the results for periodic hexagonal arrays Hex 1 and 2. The minimum INSs of -60 to -50 MPa are occurring where two fibers are almost touching perpendicular to the loading direction. It is observed in the irregular array that the maximum INSs are much higher and the minimum INSs are lower than those for periodic hexagonal arrays: the differences between the maximum and minimum INSs are respectively about 250 MPa for irregular arrays and about 150 MPa for the periodic hexagonal array.

For Case C (cooling and loading), high maximum tensile INSs of 100 to 120 MPa are occurring where two fibers are almost touching and these two fibers are parallel to the loading direction, as indicated by red solid circles. It is interesting to note that the maximum INS values for irregular fiber arrays are almost the same as those for periodic hexagonal arrays. In addition, the exact maximum INS values for Case C (100 to 120 MP) are much smaller than those for Case B (180 to 190 MPa) owing to the compensation of the compressive thermal residual INSs acting at the same locations as that of the maximum tensile mechanical INSs. Where two fibers are almost touching and their alignment is at an angle to the loading direction, the stress distribution around the shortest interfiber distance is rather mild compared to that for Case B, and the maximum INSs are not necessarily located at the shortest interfiber distance, as indicated by the red dashed circles. Thus, the INS distribution is affected by both the interfiber distance and the angle to the loading direction. This fact also agrees well with the results for periodic hexagonal arrays Hex 1 and 2. The minimum INSs of -160 to -110 MPa are occurring where two fibers are almost touching and are perpendicular to the loading direction. In this case, a large difference in the minimum values is observed among three different models. The minimum INSs for irregular arrays are much smaller than those for periodic hexagonal arrays. The difference

between the maximum and minimum INSs for irregular arrays (about 280 MPa) is thus larger than that for the periodic hexagonal arrays (about 160 MPa).

3.3 Effects of interfiber distance and fiber alignment angle for irregular fiber arrays

In this section, we define two neighboring fibers in the image-based model as a first step, and then the INSs of two neighboring fibers are quantitatively evaluated as functions of the interfiber distance and the fiber alignment angle to the loading axis. As shown in Fig. 7, each image based model is divided into Delaunay triangles using the centers of fibers [33]. Then, two neighboring fibers are defined by a pair of fibers that forms a side of a triangle. Fig. 8 indicates the local fiber distribution and the related parameters. The interfiber distance, l, is defined as the length between the two intersection points of the side of a Delaunay triangle and the fiber surfaces. The INSs at these intersection points are selected as representative INSs for evaluation in this section because INSs often have maximum or minimum values at these points. The angle between the side of a triangle and the loading direction is defined as the fiber alignment angle, θ. These two parameters, l and θ, are called the fiber distribution parameters in the present study. Then, the relationships between these representative INSs for all pairs of neighboring fibers and the fiber distribution parameters l and θ are quantitatively investigated. Since the stress distribution for fibers that have intersections with the square calculation boundary in Fig. 7 may contain errors, such fibers are not used to form Delaunay triangles and their INSs are excluded from the following processing and discussion.

Fig. 9 shows the relation between the representative INSs and the interfiber distance, l, for Case A (cooling). In this figure, open symbols show representative INSs for all fibers in the three irregular fiber array models. The solid square indicates the minimum INSs of the periodic hexagonal array, -10 MPa, at the interfiber distance of 1.6 μm. Since there are no fibers in the direction of the maximum INSs of the periodic hexagonal array, the value is indicated by an arrow. The representative INSs decrease quickly with the decrease in l

when l is smaller than 2 μm. The minimum INSs are approximately -120 MPa. The scatter of INSs is also large in this region. On the other hand, the representative INSs are from 0 to 20 MPa and their scatter is rather small when l is larger than 2 μm. It is clear that the results for the periodic hexagonal model do not represent the microscopic stress state.

Fig. 10 shows the relationship between the representative INSs and the fiber alignment angle, θ, for Case B (loading). The solid symbols indicate the maximum and minimum INSs for the periodic hexagonal arrays in Hex 1 and 2. The representative INSs increase with decreasing θ. The INSs when θ is smaller than 20˚ are high and the maximum values reach 190 MPa. The INSs become compressive when θ is 70˚ to 90˚, and the minimum values are about -50 MPa, as stated in Section 3.2. Although the scatter of the INSs is very large when θ is smaller than 45˚, it becomes rather small when θ is larger than 45˚. The minimum INSs of the periodic hexagonal arrays at θ = 60˚ and 90˚ well represent the results for the irregular fiber arrays. However, the maximum INSs at θ = 0˚ and 30˚ are within the scatter of data and are much smaller than the highest results for the irregular fiber arrays. The data for θ smaller than 20˚ are taken from Fig. 10 and plotted against l in Fig. 11. A clear relationship between the representative INSs and l is indicated in this figure, and the INSs rapidly increase up to 190 MPa when l is smaller than 0.5 μm. The change in the INSs is moderate and the INSs are about 50 to 70 MPa when l is larger than 3 μm. These values are smaller than the applied stress of 75 MPa. The solid square in this figure is the maximum INSs of the periodic hexagonal array, Hex 1, at θ = 0˚ and l = 1.6 μm. We can conclude for Case B that the maximum INSs are mainly controlled by the interfiber distance, l, and that the INSs increase with decreasing l.

Fig. 12 shows the relationship between the representative INSs and the fiber alignment angle, θ, for Case C (cooling and loading). The solid symbols indicate the maximum and minimum INSs for the periodic hexagonal arrays in Hex 1 and 2. Although the representative INSs increase with decreasing θ, the change in the INSs is small when θ is smaller than 20˚. The maximum INSs are about 120 MPa. The INSs become compressive

when θ is approximately 90˚, and the minimum values are about -160 MPa, as stated in Section 3.2. The scatter of the INSs is small when θ is smaller than 30˚, although it becomes large when θ is larger than 30˚. As was also stated in Section 3.2, the maximum INSs of the periodic hexagonal arrays at θ = 0˚ and 30˚ well represent the results for the irregular fiber arrays. However, the minimum INSs of the periodic hexagonal arrays at θ = 60˚ and 90˚ are within the scatter of data for the irregular fiber arrays. The data for θ smaller than 20˚ are taken from Fig. 12 and plotted against l in Fig. 13. The trend for the increase in the representative INSs with decreasing l disappears when l is smaller than 0.5 μm. Moreover, the INSs take a maximum of 120 MPa when l is about 0.5 μm, and after that, the INS decrease with decreasing l. The maximum INSs for Case C are much lower than those for Case B owing to the compensation of the thermal residual stresses.

This stress state also agrees well with our former in situ experiments. The interfacial failure onset was observed at the location where the interfiber distance was about 0.5 to 1 μm in the loading direction, and was not necessarily observed at the location where two fibers were almost touching [13]. The maximum INSs of 120 MPa are higher than the frequently reported bulk epoxy resin strength of 60 to 100 MPa [1,4,29,34] and the maximum value of our measurement for RTM6 using dog-bone specimens [35]. However, in our previous work we showed that a microscaled specimen of neat resin fiber has an average strength of 140 MPa for RTM6 [35]. Thus, the high calculated maximum INSs of 120 MPa, which correspond to the interfacial normal strength, are still lower than the resin strength in the microscale, and these values are acceptable. We conclude from the comparison between Cases B and C that the contribution of the thermal residual stresses in the transverse strength of CF/epoxy laminates is large, and that the stress concentration due to irregular fiber arrays does not have a detrimental effect on the transverse strength in the presence of large thermal residual stresses. These interesting results are revealed only from the complex analyses of irregular fiber arrays and detailed research on the characteristic parameters of the fiber distribution that control the microscopic stress states.

It should also be noted that the expected high transverse strength is only apparent, and that the transverse strength probably decreases when these high thermal residual stresses are released owing to, for example, environmental effects. The increases in the tangential stress and triaxial stress states due to thermal residual stresses can contribute possible matrix failure near the interface [17,18,30,31]. Then, further studies on dilatation energy or hydrostatic stress should be necessary. Another further study can be the generalization. Although the present numerical calculations apply for typical CF/epoxy systems, systematic parametric studies are also necessary in the future.

4. Conclusions

A detailed investigation has been carried out to determine the effect of local fiber array irregularities on the microscopic interfacial normal stress (INS) states for thermally and transversely loaded CF/epoxy.

(1) INSs are controlled by the fiber distribution parameters such as the interfiber length and the fiber alignment angle. High compressive INSs are observed at the location of the shortest interfiber distance when only thermal residual stresses are applied during cooling. High tensile INSs are observed at the location of the shortest interfiber distance where fibers are aligned in the loading direction when only a mechanical load is applied. The absolute values of INSs increase with decreasing interfiber distance for both cooling and mechanical loading.

(2) When both thermal and mechanical loads are applied, the thermal residual INSs suppress the high mechanical tensile INSs at the location of shortest interfiber distance where fibers are aligned to the loading direction. It is also interesting to note that the maximum INSs occur where the interfiber distance is not shortest. Thus, the microscopic thermal residual stresses contribute greatly to the increase in transverse strength.

Acknowledgements

The authors would like to thank Prof. Karl Schulte of Technical University Hamburg-Harburg, and Dr. Bodo Fielder of RUAG for their helpful discussion.

References

1 Hull D. An introduction to composite materials. Cambridge University Press, Cambridge, 1981.

2 Talreja R, editor. Damage mechanics of composite materials. Elsevier, Amsterdam, 1994.

3 Garrett KW, Bailey JE. The effect of resin failure strain on the tensile properties of glass fibre-reinforced polyester cross-ply laminates. J Materials Sci. 1977;12:2189-94.

4 Hirata M, Matsui J, Nomura S, Ishii Y. On the development of carbon fibers as reinforcement for composite materials. Proc. First Swedish-Japanese Seminar on Composite Materials, Swedish Plastics and Rubber Institute, Stockholm, 1987, pp.200-223.

5 Baron C, Schulte K, Harig H. Influence of fiber and matrix failure strain on static and fatigue properties of carbon fibre-reinforced plastics. Composite Sci. Technol. 1987;29:257-272.

6 de Kok JMM, Meijer HEM, Peijs AAJM. The influence of matrix plasticity on the failure strain of transversely loaded composite materials. Miravete A, editor, Proc. 9th International Conference on Composite Materials, Woodhead Publishing, Amsterdam, 1993, pp.242-249.

7 Schulte K, Stinchcomb WW. Damage mechanisms – including edge effects – in carbon fibre reinforced composite materials. Friedrich K, editor, Application of fracture mechanics to composite materials. Elsevier, Amsterdam, 1989, Chap. 8, pp.273-325.

8 Agarwal BD, Broutman LJ. Analysis and performance of fiber composites. John Wiley

& Sons, New York, 1990, Chap. 3, pp. 78-99.

9 Madhukar MS, Drazil LT. Fiber-matrix adhesion and its effect on composite mechanical properties: II Longitudinal (0˚) and transverse (90˚) tensile and flexure behavior of graphite/epoxy composites. J. Composite Materials 1991;25:958-991.

10 Blackketter DM, Upadhyaya D, King TR. Micromechanics prediction of the transverse tensile strength of carbon fiber/epoxy composites: The influence of the matrix and interface. Polymer Composites 1993;14:437-446.

11 de Kok JMM, Peijs T. Deformation, yield and fracture of unidirectional composites in transverse loading. 2. Influence of fibre-matrix adhesion. Composites: Part A 1999;30:917-932.

12. Norita T, Matsui J, Matsuda H. Effect of surface treatment of carbon fiber on mechanical properties of CFRP. Proc. 1st International Conference on Composite Interfaces, Cleveland, 1986, pp.2-10.

13 Hobbiebrunken T, Hojo M, Adachi T, de Jong C, Fiedler B. Evaluation of interfacial strength in CF/epoxies using FEM and in-situ experiments. Composites, Part A 2006;37:2248-2256.

14 Sjogren BA, Berglund LA. The effects of matrix and interface on damage in GRP cross-ply laminates. Composite Sci. Technol. 2000;60:9-21.

15 Sun CT, Vaidya RS. Prediction of composite properties from a representative volume element. Composite Sci. Technol. 1996;56:171-179.

16 Hobbiebrunken, T. Microscopic transverse failure initiation in composite materials – An interdisciplinary multi-scale research-. Dr. thesis, Kyoto Univesiry, 2005, Chap. 4, p.98.

17 Asp LE, Berglund LA, Talreja R. Effects of fiber and interphase on matrix-initiated transverse failure in polymer composites. Composite Sci. Technol. 1996;56:657-665.

18 Asp LE, Berglund LA, Talreja R. Prediction of matrix initiated transverse failure in polymer composites. Composite Sci. Technol. 1996;56:1089-1097.

19 Fletcher AJ, Oakeshott JL. Thermal residual microstress generation during processing of unidirectional carbon fibre/epoxy resin composites: regular fiber arrays. Composites 1994;25:797-805.

20. Sørensen BF, Talreja R. Effects of nonuniformity of fiber distribution on thermally-induced residual stresses and cracking in ceramic matrix composites. Mechanics of Materials. 1993;16:351-363.

21 Fiedler B, Hojo M, Ochiai S, Schulte K, Ochi M. Finite element modeling of initial matrix failure in CFRP under static transverse tensile load. Composite Sci. Technol. 2001;61:95-105.

22 Fletcher AJ, Oakeshott JL. Thermal residual microstress generation during processing of unidirectional carbon fibre/epoxy resin composites: random fiber arrays. Composites 1994;25:806-813.

23 Nakamura T, Suresh S. Effects of thermal residual stresses and fiber packing on deformation of metal-matrix composites. Acta Metal. Mater. 1993;41:1665-1681.

24 Bulsara VN, Talreja R, Qu J. Damage initiation under transverse loading of unidirectional composites with arbitrarily distributed fibers. Composite Sci. Technol. 1999;59:673-682.

25 Oh JH, Jin KK, Ha SK. Interfacial strain distribution of a unidirectional composite with randomly distributed fibers under transverse loading. J Composite Mat. 2006;40:759-778.

26 Jin KK, Oh JH, Ha SK. Effect of fiber arrangement on residual thermal stress distribution in a unidirectional composite. J Composite Mat. 2007;41:591-611.

27 Kishi H, Shi YB, Huang J, Yee AF. Shear ductility and toughenability study of highly cross-linked epoxy/polyethersulphone. J. Mat. Sci. 1997;32:761-771.

28 Kishi H, Shi YB, Huang J, Yee AF. Ductility and toughenability study of epoxy resins under multiaxial stress states. J. Mat. Sci. 1997;32:761-771.

29 Fiedler B, Hojo M, Ochiai S, Schulte K., Ando M. Failure behavior of an epoxy matrix

under different kinds of static loading. Composite Sci. Technol. 2001;61:1615-1624.

30 Asp LE, Berglund LA, Gudmundson P. Effects of a composite-like stress state on the fracture of epoxies. Composite Sci. Technol. 1995;53:27-37.

31 Asp LE, Berglund LA, Talreja R. A criterion for crack initiation in glassy polymers subjected to a composite-like stress state. Composite Sci. Technol. 1996;56:1291-1301.

32 Young RJ. Introduction to polymers. Chapman and Hall, London, 1987.

33 de Berg M, van Kreveld M, Overmars M, Schwarzkopf O. Computational geometry - algorithms and applications. Spriger, 2000, Chap. 9. pp.183-211.

34 Odom EM, Adams DF. Specimen size effect during tensile testing of an unreinforced polymer. J Mat. Sci. 1992;27:1767-71.

35 Hobbiebrunken T, Fiedler B, Hojo M, Tanaka M. Experimental determination of the true epoxy resin strength using micro-scaled specimens. Composites: Part A 2007;38:814-818.

Table and figures captions

Table 1. Employed values for finite element analysis.

Fig. 1. Image-based model fpr transverse loading.
(a) Original scanning electron micrograph.
(b) Image-based FE mesh for Model 1.
(c) Part of enlarged FE mesh for Model 1.

Fig. 2. SEM of cross section of composites where two fibers are almost touching (HTA/RTM6).

Fig. 3. Boundary conditions used for FE analysis.

Fig. 4. Schematic of two hexagonal models.
(a) Model Hex 1, (b) Model Hex 2

Fig. 5. Distribution of INS in hexagonal models.

(a) Case A (cooling), (b) Case B (loading) for Model Hex 1 and 2,

(c) Case C (cooling and loading) for Model Hex 1 and 2

Fig. 6. Enlarged distribution of INS for three loading cases in irregular model

(a) Case A (cooling), (b) Case B (loading), (c) Case C (cooling and loading)

Fig. 7. Delaunay triangles used to define two neighboring fibers.

Fig. 8. Interfiber distance, l, and fiber alignment angle to loading axis, θ.

Fig. 9 Relation between representative INS and interfiber distance for Case A (cooling).

Fig. 10. Relation between representative INS and fiber alignment angle for Case B (loading).

Fig. 11. Relation between representative INS and interfiber distance for Case B (loading).

Fig. 12. Relation between representative INS and fiber alignment angle for Case C (cooling and loading).

Fig. 13. Relation between representative INS and interfiber distance for Case C (cooling and loading).

Table 1. Employed values for finite element analysis.

Elastic constants

	Fiber (HTA)	Marix (RTM6)
E_{11} (GPa)	28	2.8
E_{22} (GPa)	28	2.8
E_{33} (GPa)	235	2.8
ν_{12}	0.33	0.38
ν_{23}	0.02	0.38
ν_{31}	0.28	0.38
G_{12} (GPa)	7.2	—
G_{23} (GPa)	24	—
G_{31} (GPa)	24	—

Coefficients of thermal expansion

	Fiber (HTA)	Matrix (RTM6)
α_{11}	10×10^{-6}	54×10^{-6}
α_{22}	10×10^{-6}	
α_{33}	-0.1×10^{-6}	

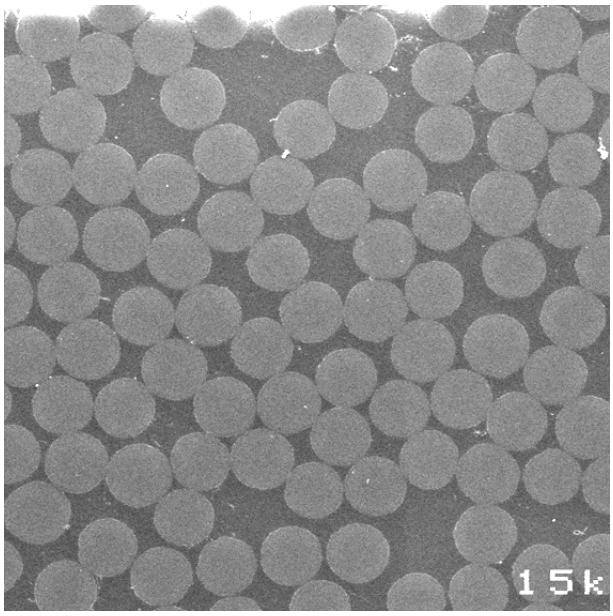

(a) Original scanning electron micrograph

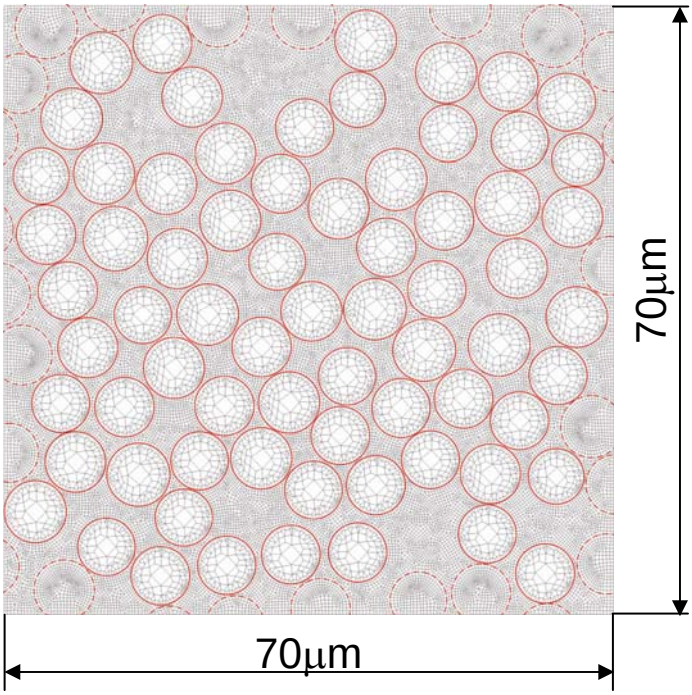

(b) Image-based FE mesh for Model 1

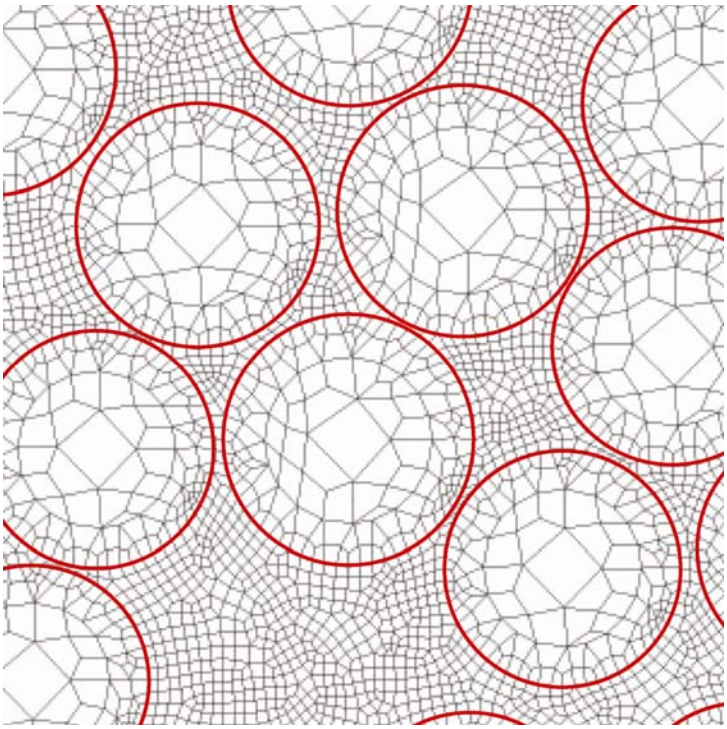

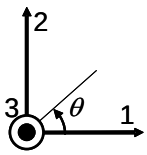

(c) Part of enlarged FE mesh for Model 1

Fig. 1. Image-based model for transverse loading.

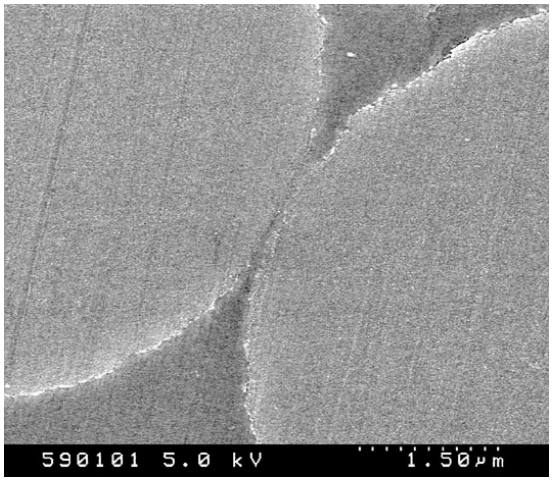

Fig. 2. SEM of cross section of composites where two fibers are almost touching (HTA/RTM6).

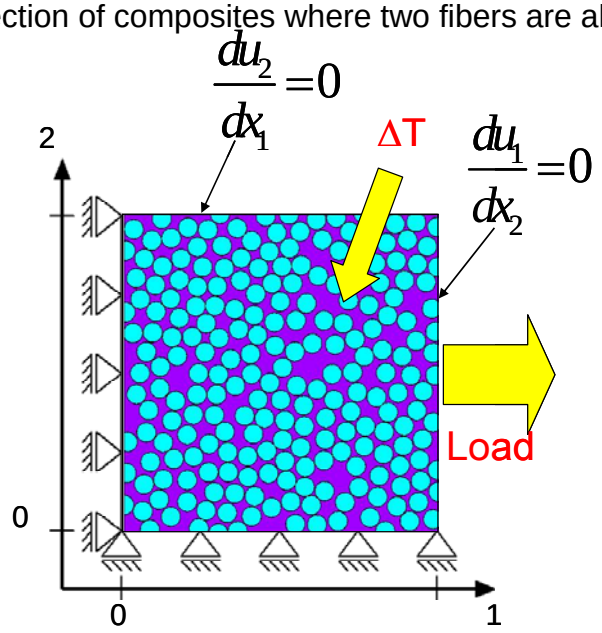

Fig. 3. Boundary conditions used for FE analysis.

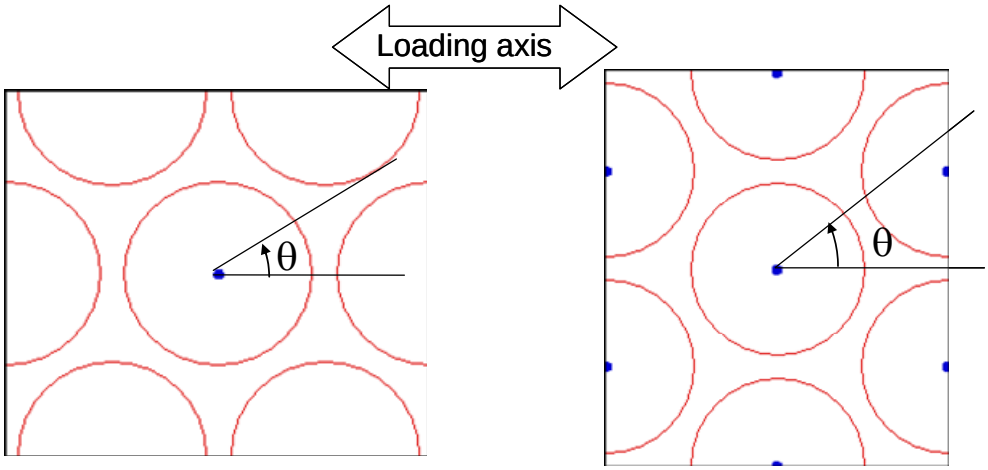

(a) Model Hex 1 (b) Model Hex 2

Fig. 4. Schematic of two hexagonal models.

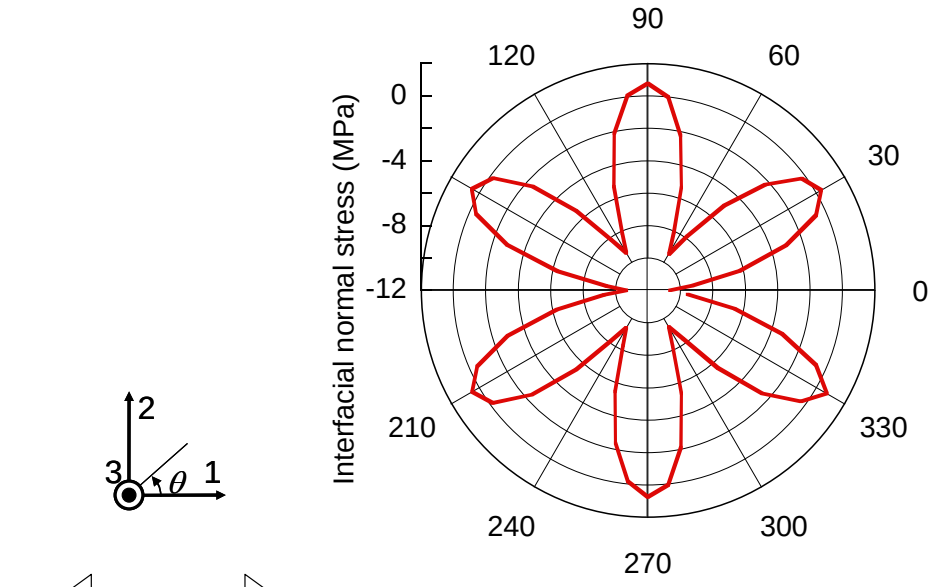

(a) Case A (cooling)

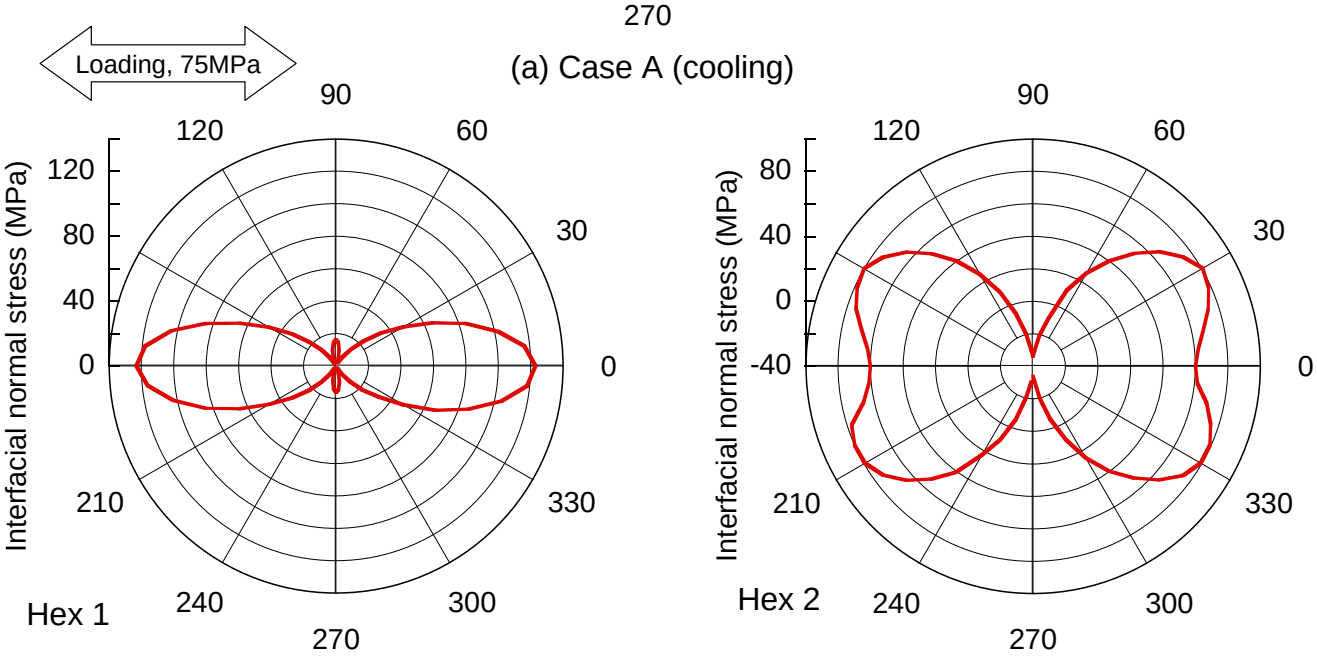

(b) Case B (loading) for Model Hex 1 and 2

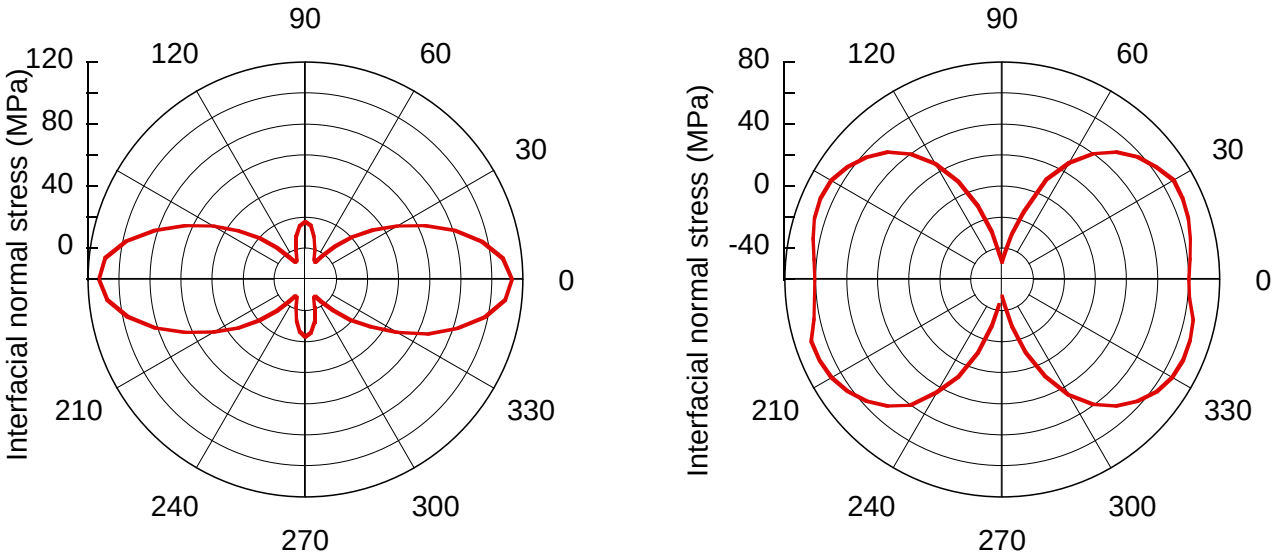

(c) Case C (cooling and loading) for Model Hex 1 and 2

Fig. 5. Distribution of INS in hexagonal models.

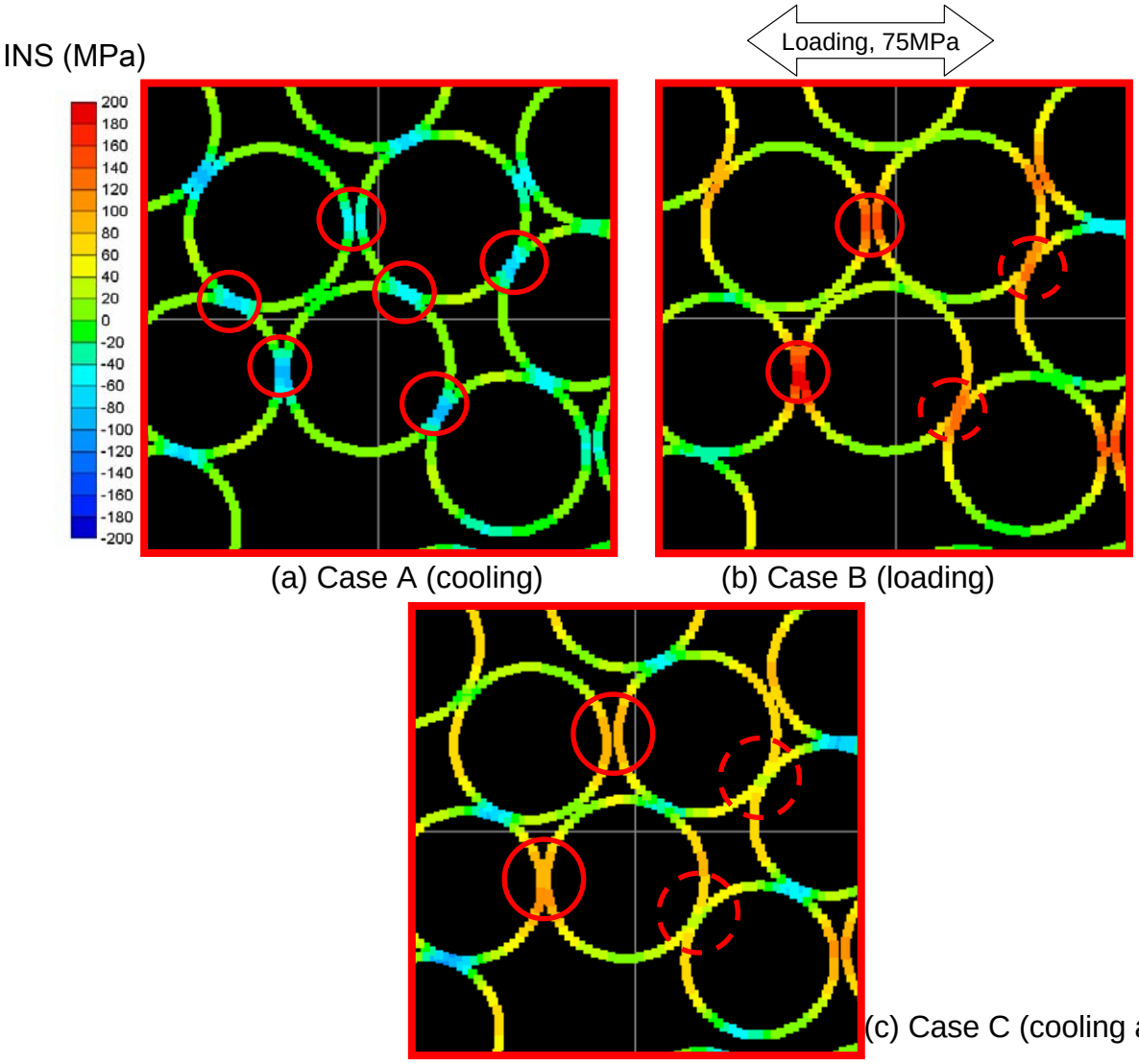

Fig. 6. Enlarged distribution of INS for three loading cases in irregular model .

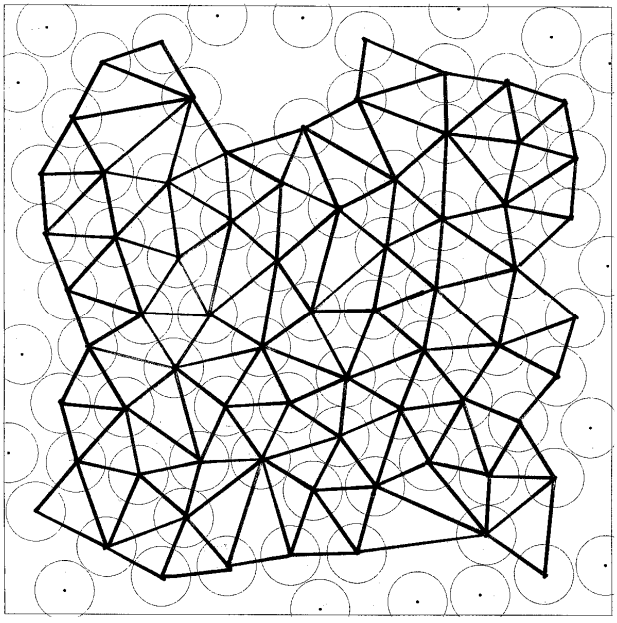

Fig. 7. Delaunay triangles used to define two neighboring fibers.

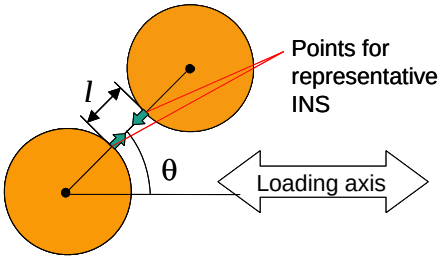

Fig. 8. Interfiber distance, *l*, and fiber alignment angle to loading axis, θ.

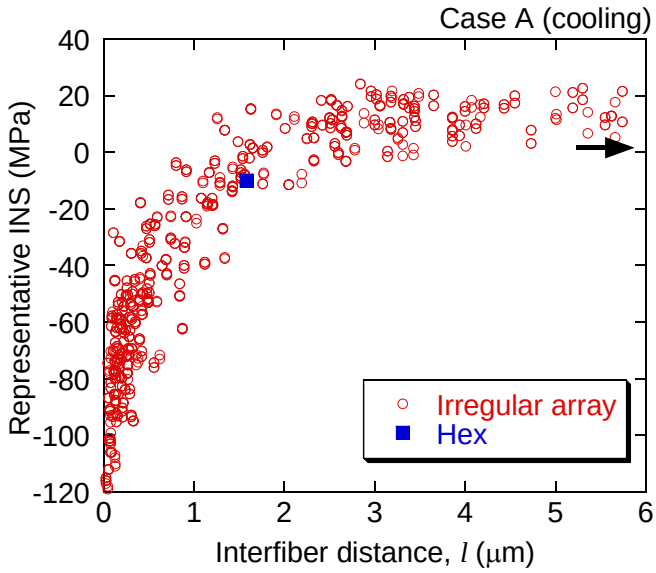

Fig. 9. Relation between representative INS and interfiber distance for Case A (cooling).

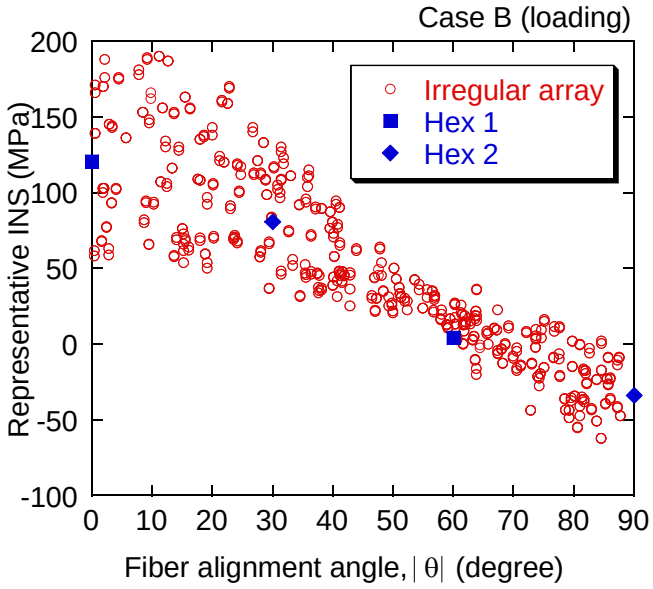

Fig. 10. Relation between representative INS and fiber alignment angle for Case B (loading).

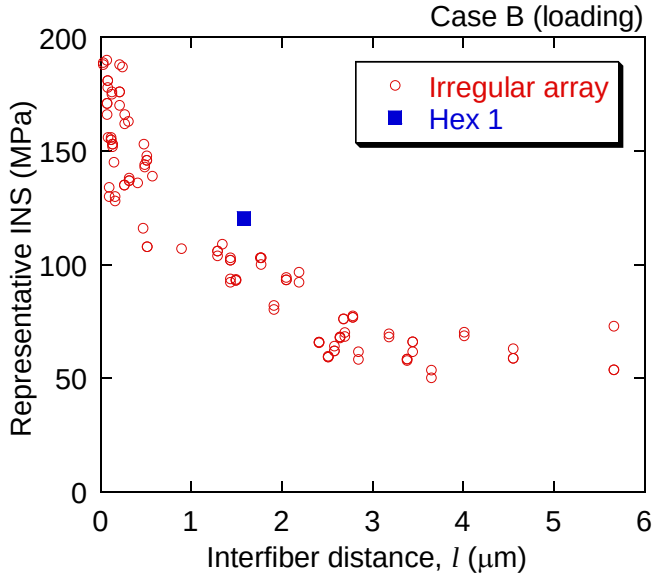

Fig. 11. Relation between representative INS and interfiber distance for Case B (loading).

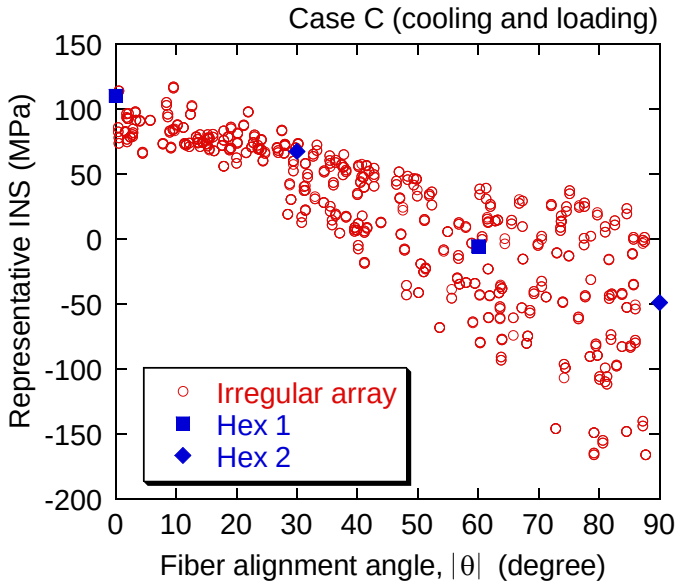

Fig. 12. Relation between representative INS and fiber alignment angle for Case C (cooling and loading).

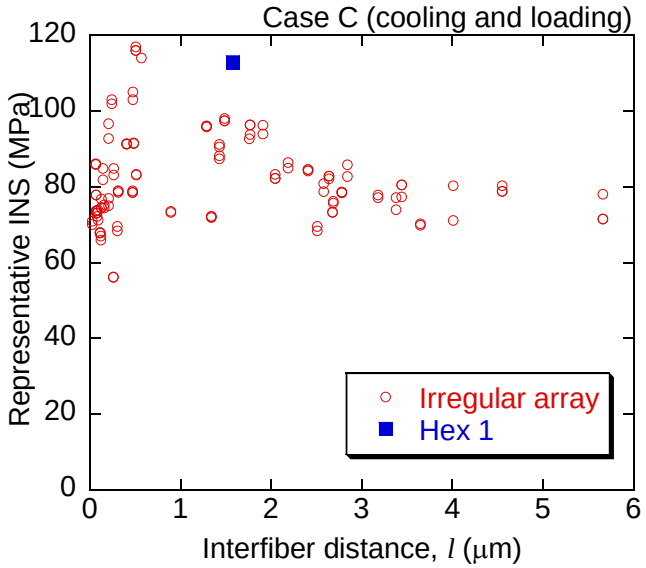

Fig. 13. Relation between representative INS and interfiber distance for Case C (cooling and loading).